ACS SENSORS

pubs.acs.org/acssensors Article

Microengineered Flexural Post Rings for Effective Blood Sample Fencing and High-Throughput Measurement of Clot Retraction Force

Lanzhu Huang, Xinyu Liu, Yuanbin Ou, Haofan Huang, Xia Zhang, Yize Wang, Yong Liang, Xiaxia Yu, Weidong Zheng, Huisheng Zhang, and Zida Li*

Cite This: https://dx.doi.org/10.1021/acssensors.0c01596 Read Online

ACCESS | Metrics & More | Article Recommendations | Supporting Information

ABSTRACT: During blood clotting, clot retraction alters its mechanical properties and critically affects hemostasis. Despite that, existing clot retraction assays hold limitations such as large footprint and low throughput. In this work, we report the design of flexural post rings for a miniaturized assay of clot retraction force (CRF) with high throughput. Leveraging surface tensions, the post rings hold blood samples in a highly reproducible fashion while simultaneously serving as cantilever beams to measure the CRF. We investigated the effect on the device performance of major parameters, namely, surface hydrophobicity, post number, and post stiffness. We then tested the devices using 14 patient samples and revealed the correlation between CRF and fibrinogen levels. We further implemented an automated liquid handler and developed a high-throughput platform for clot retraction assay. The device's small sample consumption, simple operation, and good compatibility with existing automation facilities make it a promising high-throughput clot retraction assay.

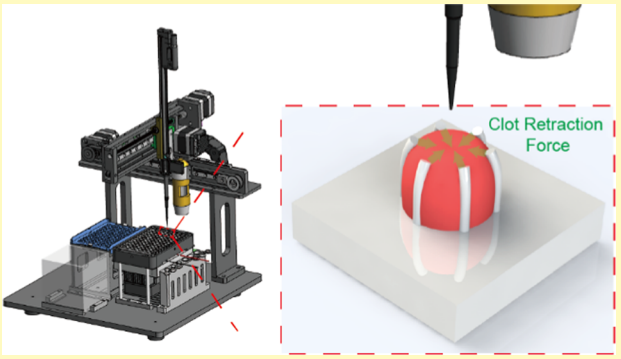

KEYWORDS: *hemostasis, clot retraction, platelet contraction, microfabrication, microengineering, high-throughput assay*

Among the leading causes of death are bleeding and thrombosis, which are induced by dysregulated blood clotting.[1] During clot formation, damaged vessel walls initiate platelet activation, aggregation, and blood coagulation, generating cross-linked fibrin meshwork with platelets embedded inside. Activated platelets generate contractile force, mediated by actin and nonmuscle myosin IIA, and compact the surrounding fibrin meshwork, leading to clot retraction.

Clot retraction has a profound impact on clotting. It reduces the clot size and consequently promotes wound closure and restoration of blood flow.[2] In addition, clot retraction alters fibrin structure and increases the stiffness of fibrin meshwork by more than 10-fold,[3] ensuring the mechanical integrity and preventing premature breakdown of the clot. Therefore, well-regulated clot retraction is critical to a balanced blood clotting, and dysregulation in clot retraction may contribute to pathological clotting. For example, it has been reported that in patients with bleeding disorders such as severe hemophilia A, clots are softer and associated with reduced stability.[3−5] The critical role of clot retraction in blood clotting is also demonstrated in patients with MYH9 defect, which compromised platelet contraction, leading to excessive bleeding and reduced clot stability, even though platelet aggregation and secretion appear normal.[2,6]

Given the significant implications of clot retraction in blood clotting, a reliable method for the characterization of clot retraction is of great importance. In early days, volume measurement was adopted in the clinics to characterize clot retraction, and similar methods are still used in fundamental researches recently.[7] The associated shortcoming of volume measurement is that it only accounts for clot morphology without factoring in clot mechanics. By monitoring clot retraction force (CRF), one could potentially discover the mechanism underlying clot formation with more details. As such, methods to measure CRF had then been developed using electronic force transducers,[8] and similar designs were later developed into a commercial instrument named Hemodyne.[9] In addition, viscoelastic hemostatic assays, such as thromboelastography (TEG) and rotational thromboelastometry (ROTEM), have been developed to measure the blood viscoelasticity during clotting, providing a means to indirectly

Received: August 2, 2020
Accepted: November 6, 2020

infer clot retraction.[10] Despite the clinical values these systems have demonstrated, they have limitations such as big footprint, high maintenance cost, and low throughput.

Microfabrication and functional materials offer the opportunity to develop miniaturized devices for clot retraction assay with low cost and high throughput.[11] Leveraging these advantages, a few devices have been developed to assess clot retraction force, including those using microposts,[12,13] atomic force microscopy,[14] traction force microscopy,[15,16] micropatterned fibrinogen array,[17] and microtissue gauge.[18] These devices had low sample consumption and high throughput with cellular-level resolution, offering great potential to elucidate the role of clot retraction in clotting. Nevertheless, the sophisticated instrument setup and complicated operation required dedicated personnel and corresponding trainings, limiting their potentials for widespread adoption.

We aim to develop a microengineered device for the assessment of clot retraction force with simple operation, low cost, and high throughput. In our previous work, we designed hanging beams for blood sample localization and force sensing.[19,20] Despite the success in CRF measurement, the devices required attentive and skilled manual pipetting, which limits their adaptation in automated high-throughput *in vitro* diagnostics. To address this problem, in this work, we designed flexural post rings (FPR) using soft materials to localize blood sample and simultaneously measure the generated clot retraction force. The FPR served as a fence for easy blood sample loading, and surface tension ensured that blood samples were localized in a reproducible manner, which allows assay automation using liquid handlers. As the blood was clotting, the clot deflected the posts and the CRF was calculated based on the displacement of the post tips. We investigated the effect of surface hydrophobicity, post numbers, and post stiffness on the measurement. To validate the measurements from FPR, we tested blood samples from 14 patients and found a correlation between the measured CRF and fibrinogen level. We further accommodated FPR with a customized liquid handling platform for automated blood sample loading and subsequent CRF testing, demonstrating the great potential of FPR in high-throughput *in vitro* clotting diagnostics. FPR's low cost, small sample consumption, simple operation, and good compatibility with existing automation facilities make it a promising clot retraction assay.

METHODS

Device Design and Fabrication. FPR devices were made of poly(dimethylsiloxane) (PDMS) through replica molding. Briefly, the negative image of the designed pattern was first generated on acrylic sheets using laser cutting (V2000, Diyi Optoelectronics Company), before the acrylic sheet was adhered to a Petri dish and served as the mold. PDMS prepolymer (Sylgard 184, Dow, Inc.), with a 20:1 base-to-hardener ratio, was poured into the Petri dish, degassed, and baked in a 60 °C oven for 10 h, before being peeled off and cut into desired size. When studying the effect of surface hydrophobicity on sample confinement, the surface of FPR was additionally treated with oxygen plasma using a plasma cleaner (PT38-220V-40KHZ, Sanheboda Company) for specified durations.

Blood Specimen. Whole blood samples were collected from human volunteers into blue-top vacutainer tubes (Improvacuter, Improve Medical; 3.8% sodium citrate) and processed under a protocol approved by the Institutional Review Board in Health Science Center at Shenzhen University. All blood samples were tested within 4 h after blood draw. Fibrinogen levels were tested using an optical detection method on a commercial instrument (CS-5100 Hemostasis System, Sysmex Corporation).

Experimental Setup. In initial experiments, clot retraction tests were performed in a lab-made acrylic box equipped with a temperature controller (TC-05B, Xifa Electronics) and strip heater (Model 60227, Baohing Electric Wire & Cable Co.), at a set temperature of 37 °C. Citrated blood samples were supplemented with 0.2 M $CaCl_2$ (Sigma-Aldrich Co.) with a volume ratio of 17:1, before 4.5 μL of the recalcified samples were loaded into the FPR devices. Image acquisition was then started using a stereomicroscope coupled with a CCD camera (SMZ-171T, Motic China Group Co.).

In the high-throughput assay, a customized liquid handling platform was developed for automatic sample loading. Briefly, an electronic pipetting module was used for sample loading, a digital microscope (Dino-Lite AM4113T, AnMo Electronics Corporation) was used for image acquisition, and motorized stages were used for the movement of the pipette and microscope. A reagent racks, a pipette box, and a tip bin were also incorporated. In addition, a heating module was embedded into the testing stage to provide desirable testing temperatures. To calibrate the pipetting volume, a balance with a precision of 0.1 mg (ME204E, Mettler Toledo, LLC) was used to weigh the dispensed water droplet.

Simulation and Data Analysis. Simulation of the post bending was performed using a stationary solid mechanics model in COMSOL Multiphysics. The Young's modulus, Poisson's ratio, and density of the PDMS were 300 kPa, 0.49, and 970 kg/m^3, respectively.[19] A uniformly distributed force was applied on one side of the post, and the displacement of the tip of the post was obtained from the simulation result. By applying a series of loads, a series of displacements were obtained correspondingly, which were used to calculate the effective spring constant of the post.

Clot retraction forces were calculated by image analysis in Python. Briefly, images were first cropped to isolate the posts, before the cropped images were flattened into grayscale, thresholded into binary, and analyzed to find the contours of the tips (Figure S3). Minimum enclosing circles of contours were then calculated, and the centroids of the circles were reported as the coordinates of the tips of the posts. Displacements of the posts were subsequently calculated and used to deduce clot retraction force. Circularity of the placed blood drops was defined as $4\pi \times \text{area/perimeter}^2$ and analyzed in ImageJ. Contact angles were measured by capturing images with a camera coupled with a zoom lens (AF-S VR Zoom-Nikkor, Nikon, Inc.) and analyzing the images in ImageJ (NIH).

RESULTS

Overview of the Device Design. The device of flexural post rings (FPR) consists of a set of flexural posts arranged as a circle, forming a fence to spatially confine a drop of blood sample. As a blood drop is dispensed inside of the FPR, surface tension tends to minimize the surface area, leading the blood drop to an equilibrium position and shape in a reproducible manner (Figure 1a,b). When the blood drop is clotting and contracting, the clot exerts force on the posts, bending the posts toward the center (Figure 1c). By monitoring the displacements of the posts, the clot retraction force (CRF) can be calculated based on the structural stiffness of the posts.

We developed a fabrication protocol of the FPR device based on PDMS replica molding, where the mold was fabricated by laser cutting acrylic sheet (see the Methods section; Figure S1). This fabrication protocol ensured that the devices were generated in a reproducible and cost-effective manner. To model the structural stiffness of the posts, we performed simulation of structural mechanics (Figure 1d,e). As we applied various loads on a side of the post, the post tip exhibited a displacement, which was linearly responsive to the amplitude of the load; the load-displacement data were then used to calculate the spring constant (Figure 1e). For example, with a height of 1.5 mm and a diameter of 0.25 mm, the calculated spring constant was 0.247 μN/μm. Posts with

https://dx.doi.org/10.1021/acssensors.0c01596
ACS Sens. XXXX, XXX, XXX−XXX

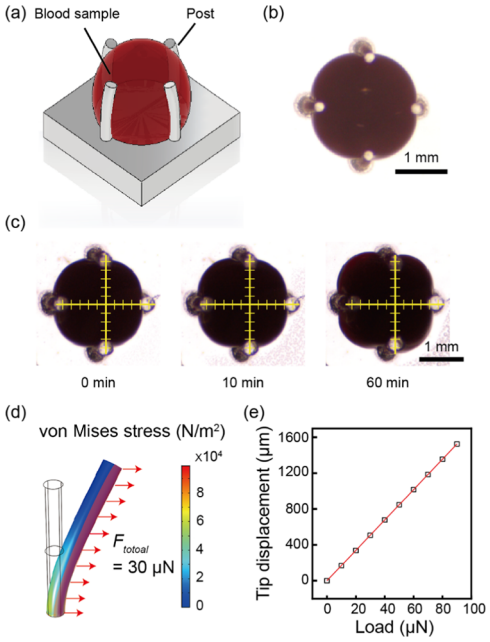

Figure 1. (a) Schematic of the device for clot retraction force measurement. Vertical flexible posts are adopted to confine a blood drop inside the post ring and simultaneously gauge the clot retraction force like cantilever beams. (b) Micrograph of the device during measurement. (c) Representative micrograph sequence showing the dynamics of clot retraction and post bending. (d) Simulation of the structural mechanics of the post deformation. The applied load in this case was 30 μN. (e) Displacement of the post tip as a function of the load as computed from simulation (black squares). The spring constant of the post is then calculated by linear fitting (red line).

different heights and diameters were modeled, and the calculated spring constants were tabulated for later use (Figure S2).

In the clot retraction test, citrated blood samples were first recalcified, before 4.5 μL of the samples were immediately loaded into FPR devices. Images were then acquired and analyzed to obtain displacements and CRF (Figure S3), generating results with post-to-post variations typically around 15%. We additionally performed the assay using citrated blood samples without recalcification as a negative control. As shown in Figure 2, with the recalcified blood sample, CRF developed rapidly in the initial stage, and at about 40 min, the force development slowed down and the CRF reached a plateau of about 40 μN. In contrast, with the citrated blood sample, the displayed forces were generally lower than 10 μN, which was significantly smaller. The nonzero results were likely due to the minute evaporation of the blood sample during the test. These results confirmed that the reported force was indeed induced by clot retraction.

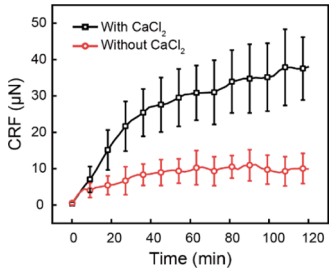

Figure 2. Clot retraction force (CRF) measured from citrated blood supplemented with and without $CaCl_2$. Calcium neutralizes citrate and triggers blood coagulation. Data represent mean ± SD with n = 3.

We then compared the measurements using FPR devices with reported results using the commercialized instrument Hemodyne.[9] We normalized the measured force over the volume of blood sample for comparison. Calculation showed that the force per unit blood volume was 9.7 ± 0.6 μN/μL using FPR devices and 66.8 ± 4.7 μN/μL using Hemodyne (Table S1). The force measured using Hemodyne was about 7 times of that measured using our devices. A contributing factor to this difference could be that the protocol of Hemodyne used batroxobin, which activated platelets to obtain maximal contraction. In addition, the difference in other experimental setups such as clot geometry could have also contributed to this difference in measurement.

Characterization of the FPR Device. The performance of the FPR device relied predominantly on design parameters including the hydrophobicity of the surface and the geometry of the post rings, such as post number and stiffness. We characterized the effect of these parameters on sample loading and CRF measurement, aiming to find the parameter values with optimal device performance.

Surface hydrophobicity affects the confinement as well as the localization of the blood drop inside the FPR. Intuitively, nonwetting surfaces with relatively high contact angles would be beneficial to drop confinement. To test that, we treated PDMS with oxygen plasma for different durations to obtain surfaces with various contact angles (Figure S4) and investigated the blood drop localization performance. The results showed that hydrophobic surface was indeed favorable to sample loading and localization, as demonstrated in Figure 3a. For example, plain PDMS without oxygen plasma treatment, which had a contact angle of 122.4°, exhibited good drop confinement. As we gradually increased the treatment time and reduced the contact angle, the blood drop was well contained by the post rings up until 2 s of treatment with a contact angle of 75.6°. With 3 s of treatment, where contact angle was 42.3°, blood drop slightly invaded out of FPR, and with 4 s of treatment, where contact angle was 32.7°, surface tension was no longer able to confine the blood drop and it spread out of the FPR. Blood drops spread even further on surfaces with even lower contact angles. These results showed that for effective sample loading, contact angles higher than 75° are desirable.

Post number is another factor that affects the drop confinement. To have the blood drop loaded in a stable position and thus a reproducible manner, we aim to obtain a blood drop in a circular shape with minimized surface energy. More posts provide more anchors and thus more surface tension, leading the drop to a more symmetric and stable shape at equilibrium. Indeed, with three posts, the drop adopted a less circular shape on the vertical projection, with a calculated circularity of 0.848 ± 0.022. As we added more posts, the drop shape on vertical project became more circular. With four posts, the shape was almost a circle, with a circularity of 0.888 ± 0.013, which was significantly larger than that of three posts. As we added more posts, the change in the circularity became less significant, and the circularity maintained around 0.90. However, the variations were lowered with more posts, indicating that a higher post number could lead to better reproducibility in the drop shape. As such, designs with at least six posts were used in the following experiments.

https://dx.doi.org/10.1021/acssensors.0c01596
ACS Sens. XXXX, XXX, XXX−XXX

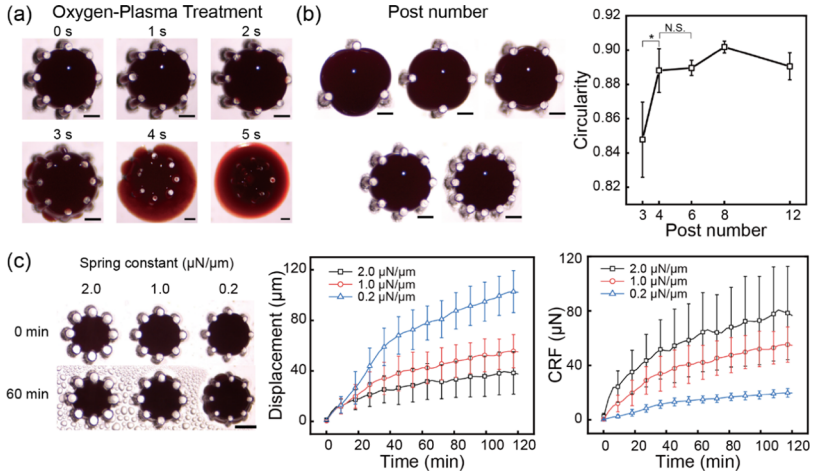

Figure 3. Characterization of the effect of surface hydrophobicity, post amount, and post stiffness on sample loading and test results. (a) Representative micrographs of sample localization on devices treated with oxygen plasma of different doses as indicated. Scale bars, 500 μm. (b) Representative micrographs of sample localization on devices with different post numbers and the calculated circularity. Scale bars, 500 μm. (c) Micrographs of tests, displacement tracings, and CRF tracings using posts with different spring constants. Scale bar, 1 mm. Data represent mean ± SD with n = 3.

We then characterized the effect of beam stiffness on the CRF measurement. By adjusting the diameter of the posts while adopting a constant post height, we obtained spring constants of 0.2, 1.0, and 2.0 μN/μm, as determined by simulations of the structural mechanics (Figure S2). Results showed that soft posts generated more displacements, as shown in Figure 3c. For example, posts with a spring constant of 0.2 μN/μm exhibited a displacement of 102.7 ± 16.6 μm at the end of the assays, which were almost 3-fold of that using posts with a spring constant of 2.0 μN/μm. This observation could be explained by the fact that soft posts were more prone to deformations and thus showed more bending. However, the calculated CRF displayed an inverse trend: soft posts generated less CRF. For example, the CRF at the end of the assays using posts with a spring constant of 0.2 μN/μm was 19.8 ± 3.2 μN, which were roughly one-fourth of that using posts with a spring constant of 2.0 μN/μm. This observation was likely induced by the mechanosensitive nature of platelets. Contractile forces generated by platelets are dependent on the mechanical properties of the environment.[21] It has been shown that higher substrate stiffness promotes platelet adhesion and spreading, and substrate stiffness also mediates platelet activation,[22] which in turn affects platelet contractile force.[23] In addition, it is well recognized that platelet contraction modulates the stiffness of the clot.[24] Based on these reported findings, a possible explanation for our observation is that clots on posts with different bending stiffnesses first exhibit different levels of contraction, which modulates the stiffness of the clot itself, and the differential stiffness of the clot further affects the contractility of the platelets within the clot. Consequently, clots on posts of different spring constants showed different levels of retraction force. This observation also implied that the stiffness of force-sensing probes should be carefully controlled when designing clot retraction assays to ensure that variables are well controlled.

Preliminary Validation of the Assay. As a first step toward clinical validation of FPR devices, we performed clot retraction tests using FPR devices on blood samples from 14 volunteers. In addition, we measured the fibrinogen levels of these samples using standard clinical tests (see the Methods section) for references. Fibrinogen level affects the mechanical microenvironment of platelets and the mechanical integrity of the cross-linked fibrin meshwork,[25,26] and thus higher fibrinogen levels could be correlated to elevated CRF. As shown in Figure 4, FPR successfully captured the dynamic

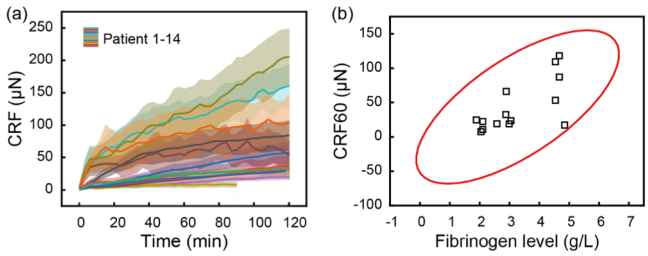

Figure 4. CRF measurements from 14 patients. (a) CRF tracings of different patients. Shades represent SD with n = 3. (b) Correlation between the measured CRF at 60 min (CRF60) and fibrinogen levels. The red ellipse indicates 95% confidence. Pearson's correlation coefficient was calculated as 0.69 with P < 0.01.

CRF curves of all of the patients and revealed a large range of CRF values. To quantitatively compare the CRF measurement with fibrinogen level, we extracted the CRF at 60 min, denoted as CRF60, as a characteristic CRF amplitude and performed correlation analysis with fibrinogen levels. The results showed that CRF60 had a strong correlation with fibrinogen levels, with a Pearson's correlation of 0.69 (P < 0.01), indicating that elevated CRF values might be associated with elevated fibrinogen levels. This result suggested the clinical applicability of FPR devices.

High-Throughput Testing Platform. The ease and high reproducibility of sample loading equipped FPR devices with the potential for the development of automated, high-throughput clot retraction assays. To demonstrate that, we designed and implemented a liquid handling platform to realize automated sample loading and image acquisition (Video S1). As shown in Figure 5a, the platform was mainly composed of motorized linear stages, an electronic pipetting module, and a digital microscope. The motorized stages moved on the X−Y plane for pipette tip and camera positioning, as well as on the Z

https://dx.doi.org/10.1021/acssensors.0c01596
ACS Sens. XXXX, XXX, XXX−XXX

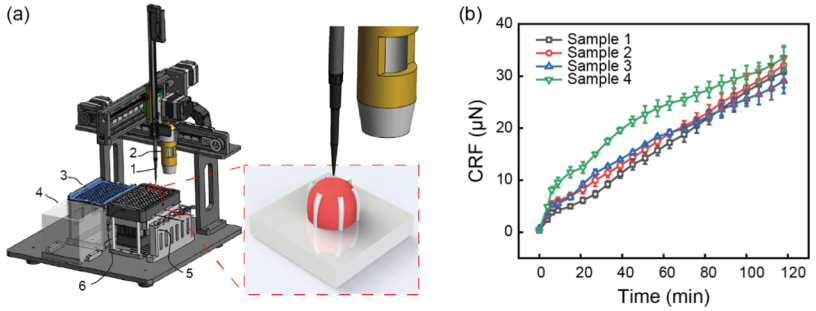

Figure 5. Automated testing platform using a customized liquid handler. (a) Schematic of the liquid handler and testing stage: (1) electronic pipetting module; (2) digital microscope; (3) pipette tip box; (4) ejected tip bin; (5) sample and reagent rack; (6) testing stage with embedded heater. (b) CRF tracings from four different samples measured with the automated platform. Data represent mean ± SD with $n = 4$.

axis for liquid dispensing. The electronic pipetting module performed tip loading, tip ejection, and blood sample pipetting. The module was carefully calibrated to achieve precise liquid dispensing, with the coefficient of variation of the volume less than 4% in our target volume range (Table S2). FPR devices were placed in a 12-well cell plate to assist positioning and alleviate evaporation.

Using the high-throughput testing platform, we performed clot retraction assays on four blood samples simultaneously. Each sample was tested on four FPR devices to average out device-induced variations, and the pipetting process adopted a single-aspiration, multiple-dispensing practice to improve the pipetting efficiency. As a result, the platform was able to finish sample loading into FPR devices within 15 s for each sample (see Video S1). The CRF curves were successfully acquired with little human intervention, and consistent results were observed (Figure 5b). By upgrading the translation stage with faster motion, we could potentially achieve a higher sample loading speed. These results demonstrated the great application potential of the FPR devices for high-throughput *in vitro* clotting diagnostics.

DISCUSSION AND CONCLUSIONS

In this work, we presented the design of flexural post rings for clot retraction force measurement with easy sample loading, low cost, and good compatibility with automated *in vitro* diagnostics facilities. The post rings provided fences to confine blood drops inside while simultaneously measuring the clot retraction force. We investigated the effect of major parameters on the device performance and conducted the assays on patient samples. The assay results showed positive correlation with fibrinogen levels, suggesting the device's clinical validity. We further implemented an automated liquid handler and developed a high-throughput clot retraction testing platform. Compared to existing methods for clot retraction measurement such as traction force microscopy, this device only requires a zoom-in camera for data acquisition, as opposed to the dedicated fluorescence imaging equipment. In addition, the compatibility with liquid handling platform enables high-throughput assay development. These advantages equipped the device with the potential to be served as a clot retraction assay with great clinical applications.

Nevertheless, we should note that a few limitations shall be addressed in future work. First, the current form of the device uses still blood samples. In physiological settings, blood clots are constantly exposed to hemodynamic shear. Though clot retraction assays using still blood samples have shown good applicability,[9] incorporation of shear flow in the measurement can better recapitulate the clotting process and thus provide a more physiologically relevant measurement. Second, given that the sample measurement is sensitive to posts' spring constant, it is important to have good quality control on the fabrication process to make sure variables in the measurements are controlled. In addition, future work could be devoted to unveiling the underlying mechanism of the influence of posts' stiffness on clot retraction. Such studies can provide insights from mechanistic perspectives and guide future designs of clot retraction assays.

ASSOCIATED CONTENT

Supporting Information

The Supporting Information is available free of charge at https://pubs.acs.org/doi/10.1021/acssensors.0c01596.

Fabrication process, spring constant simulations, image processing algorithm, contact angles, measurement comparison, and electronic pipetting module calibration (PDF)

Sample loading and automated imaging (MP4)

AUTHOR INFORMATION

Corresponding Author

Zida Li − *Department of Biomedical Engineering, School of Medicine and Guangdong Key Laboratory for Biomedical Measurements and Ultrasound Imaging, Department of Biomedical Engineering, School of Medicine, Shenzhen University, Shenzhen 518060, China;* orcid.org/0000-0002-1353-9414; Email: zidali@szu.edu.cn

Authors

Lanzhu Huang − *Department of Biomedical Engineering, School of Medicine and Guangdong Key Laboratory for Biomedical Measurements and Ultrasound Imaging, Department of Biomedical Engineering, School of Medicine, Shenzhen University, Shenzhen 518060, China*

Xinyu Liu − *Department of Biomedical Engineering, School of Medicine and Guangdong Key Laboratory for Biomedical Measurements and Ultrasound Imaging, Department of Biomedical Engineering, School of Medicine, Shenzhen University, Shenzhen 518060, China; Faculty of Information Technology, Collaborative Laboratory for Intelligent Science and Systems and State Key Laboratory of Quality Research in Chinese Medicines, Macau University of Science and Technology, Macao 999078, China*

Yuanbin Ou − *Department of Biomedical Engineering, School of Medicine and Guangdong Key Laboratory for Biomedical*

https://dx.doi.org/10.1021/acssensors.0c01596
ACS Sens. XXXX, XXX, XXX−XXX

Measurements and Ultrasound Imaging, Department of Biomedical Engineering, School of Medicine, Shenzhen University, Shenzhen 518060, China

Haofan Huang − *Department of Biomedical Engineering, School of Medicine and Guangdong Key Laboratory for Biomedical Measurements and Ultrasound Imaging, Department of Biomedical Engineering, School of Medicine, Shenzhen University, Shenzhen 518060, China*

Xia Zhang − *Department of Laboratory Medicine, Shenzhen University General Hospital, Shenzhen 518055, China*

Yize Wang − *Department of Mechanical and Process Engineering, ETH Zurich, 8092 Zurich, Switzerland*

Yong Liang − *Faculty of Information Technology, Collaborative Laboratory for Intelligent Science and Systems and State Key Laboratory of Quality Research in Chinese Medicines, Macau University of Science and Technology, Macao 999078, China*

Xiaxia Yu − *Department of Biomedical Engineering, School of Medicine and Guangdong Key Laboratory for Biomedical Measurements and Ultrasound Imaging, Department of Biomedical Engineering, School of Medicine, Shenzhen University, Shenzhen 518060, China*

Weidong Zheng − *Department of Laboratory Medicine, Shenzhen University General Hospital, Shenzhen 518055, China*

Huisheng Zhang − *Department of Biomedical Engineering, School of Medicine and Guangdong Key Laboratory for Biomedical Measurements and Ultrasound Imaging, Department of Biomedical Engineering, School of Medicine, Shenzhen University, Shenzhen 518060, China*

Complete contact information is available at: https://pubs.acs.org/10.1021/acssensors.0c01596

Author Contributions

L.H. and X.L. contributed equally. L.H. fabricated the devices, performed the assays, and analyzed the data. X.L., Y.O., Y.L., and H.Z. designed the liquid handler and contributed to the assays. H.H. and X.Y. wrote the program for image analysis. Y.W. built 3D models and performed simulations. X.Z. and W.Z. collected blood samples and contributed to assay designs. Z.L. designed the project, supervised the execution, analyzed the data, and wrote the manuscript. All authors commented on the manuscript.

Notes

The authors declare no competing financial interest.

■ ACKNOWLEDGMENTS

The authors thank Xiaoxue Yao and Prof. Tiantian Kong for the assistance with the measurement of contact angles. This work was supported by the Natural Science Foundation of Guangdong Province (2019A1515012010), Guangdong Committee of Hygiene and Health (A2019492), Shenzhen Overseas Talent Program, and Shenzhen University Faculty Startup Grant (2019132).

■ REFERENCES

(1) World Health Organization. Fact Sheets of Cardiovascular Diseases (CVDs). https://www.who.int/en/news-room/fact-sheets/detail/cardiovascular-diseases-(cvds) (accessed March 15, 2020).

(2) Tutwiler, V.; Litvinov, R. I.; Lozhkin, A. P.; Peshkova, A. D.; Lebedeva, T.; Ataullakhanov, F. I.; Spiller, K. L.; Cines, D. B.; Weisel, J. W. Kinetics and mechanics of clot contraction are governed by the molecular and cellular composition of the blood. *Blood* **2016**, *127*, 149−159.

(3) Lam, W. A.; Chaudhuri, O.; Crow, A.; Webster, K. D.; Li, T. D.; Kita, A.; Huang, J.; Fletcher, D. A. Mechanics and contraction dynamics of single platelets and implications for clot stiffening. *Nat. Mater.* **2011**, *10*, 61−66.

(4) Lisman, T.; Mosnier, L. O.; Lambert, T.; Mauser-Bunschoten, E. P.; Meijers, J. C.; Nieuwenhuis, H. K.; de Groot, P. G. Inhibition of fibrinolysis by recombinant factor VIIa in plasma from patients with severe hemophilia A. *Blood* **2002**, *99*, 175−179.

(5) Hvas, A. M.; Sørensen, H. T.; Norengaard, L.; Christiansen, K.; Ingerslev, J.; Sørensen, B. Tranexamic acid combined with recombinant factor VIII increases clot resistance to accelerated fibrinolysis in severe hemophilia A. *J. Thromb. Haemostasis* **2007**, *5*, 2408−2414.

(6) Léon, C.; Eckly, A.; Hechler, B.; Aleil, B.; Freund, M.; Ravanat, C.; Jourdain, M.; Nonne, C.; Weber, J.; Tiedt, R.; Gratacap, M.-P.; Severin, S.; Cazenave, J.-P.; Lanza, F.; Skoda, R.; Gachet, C. Megakaryocyte-restricted MYH9 inactivation dramatically affects hemostasis while preserving platelet aggregation and secretion. *Blood* **2007**, *110*, 3183−3191.

(7) Tutwiler, V.; Peshkova, A. D.; Le Minh, G.; Zaitsev, S.; Litvinov, R. I.; Cines, D. B.; Weisel, J. W. Blood clot contraction differentially modulates internal and external fibrinolysis. *J. Thromb. Haemostasis* **2019**, *17*, 361−370.

(8) Cohen, I.; de Vries, A. Platelet contractile regulation in an isometric system. *Nature* **1973**, *246*, 36.

(9) Carr, M. E. Development of platelet contractile force as a research and clinical measure of platelet function. *Cell Biochem. Biophys.* **2003**, *38*, 55−78.

(10) Chen, A.; Teruya, J. Global hemostasis testing thromboelastography: old technology, new applications. *Clin. Lab. Med.* **2009**, *29*, 391−407.

(11) Li, X.; Chen, W.; Li, Z.; Li, L.; Gu, H.; Fu, J. Emerging microengineered tools for functional analysis and phenotyping of blood cells. *Trends Biotechnol.* **2014**, *32*, 586−594.

(12) Liang, X. M.; Han, S. J.; Reems, J.-A.; Gao, D.; Sniadecki, N. J. Platelet retraction force measurements using flexible post force sensors. *Lab Chip* **2010**, *10*, 991−998.

(13) Ting, L. H.; Feghhi, S.; Taparia, N.; Smith, A. O.; Karchin, A.; Lim, E.; John, A. S.; Wang, X.; Rue, T.; White, N. J.; et al. Contractile forces in platelet aggregates under microfluidic shear gradients reflect platelet inhibition and bleeding risk. *Nat. Commun.* **2019**, *10*, No. 1204.

(14) Lam, W. A.; Chaudhuri, O.; Crow, A.; Webster, K. D.; Kita, A.; Huang, J.; Fletcher, D. A.; et al. Mechanics and contraction dynamics of single platelets and implications for clot stiffening. *Nat. Mater.* **2011**, *10*, 61−66.

(15) Henriques, S. S.; Sandmann, R.; Strate, A.; Köster, S. Force field evolution during human blood platelet activation. *J. Cell Sci.* **2012**, *125*, 3914−3920.

(16) Hanke, J.; Ranke, C.; Perego, E.; Köster, S. Human Blood Platelets Contract in Perpendicular Direction to Shear Flow. *Soft Matter* **2019**, *15*, 2009−2019.

(17) Myers, D. R.; Qiu, Y.; Fay, M. E.; Tennenbaum, M.; Chester, D.; Cuadrado, J.; Sakurai, Y.; Baek, J.; Tran, R.; Ciciliano, J. C.; Ahn, B.; Mannino, R. G.; Bunting, S. T.; Bennett, C.; Briones, M.; Fernandez-Nieves, A.; Smith, M. L.; Brown, A. C.; Sulchek, T.; Lam, W. A. Single-platelet nanomechanics measured by high-throughput cytometry. *Nat. Mater.* **2017**, *16*, 230−235.

(18) Chen, Z.; Lu, J.; Zhang, C.; Hsia, I.; Yu, X.; Marecki, L.; Marecki, E.; Asmani, M.; Jain, S.; Neelamegham, S.; et al. Microclot array elastometry for integrated measurement of thrombus formation and clot biomechanics under fluid shear. *Nat. Commun.* **2019**, *10*, No. 2051.

(19) Li, Z.; Li, X.; McCracken, B.; Shao, Y.; Ward, K.; Fu, J. A miniaturized hemoretractometer for blood clot retraction testing. *Small* **2016**, *12*, 3926−3934.

(20) Li, Z.; Wang, Y.; Xue, X.; McCracken, B.; Ward, K.; Fu, J. Carbon Nanotube Strain Sensor Based Hemoretractometer for Blood Coagulation Testing. *ACS Sens.* **2018**, *3*, 670−676.
(21) Qiu, Y.; Brown, A. C.; Myers, D. R.; Sakurai, Y.; Mannino, R. G.; Tran, R.; Ahn, B.; Hardy, E. T.; Kee, M. F.; Kumar, S.; Bao, G.; Barker, T. H.; Lam, W. A. Platelet mechanosensing of substrate stiffness during clot formation mediates adhesion, spreading, and activation. *Proc. Natl. Acad. Sci. U.S.A.* **2014**, *111*, 14430−14435.
(22) Qiu, Y.; Brown, A. C.; Myers, D. R.; Sakurai, Y.; Mannino, R. G.; Tran, R.; Ahn, B.; Hardy, E. T.; Kee, M. F.; Kumar, S.; et al. Platelet mechanosensing of substrate stiffness during clot formation mediates adhesion, spreading, and activation. *Proc. Natl. Acad. Sci. U.S.A.* **2014**, *111*, 14430−14435.
(23) Myers, D. R.; Qiu, Y.; Fay, M. E.; Tennenbaum, M.; Chester, D.; Cuadrado, J.; Sakurai, Y.; Baek, J.; Tran, R.; Ciciliano, J. C.; et al. Single-platelet nanomechanics measured by high-throughput cytometry. *Nat. Mater.* **2017**, *16*, 230.
(24) Jen, C. J.; McIntire, L. V. The structural properties and contractile force of a clot. *Cell Motil.* **1982**, *2*, 445−455.
(25) Qiu, Y.; Ciciliano, J.; Myers, D. R.; Tran, R.; Lam, W. A. Platelets and physics: How platelets "feel" and respond to their mechanical microenvironment. *Blood Rev.* **2015**, *29*, 377−386.
(26) Tutwiler, V.; Peshkova, A. D.; Andrianova, I. A.; Khasanova, D. R.; Weisel, J. W.; Litvinov, R. I. Contraction of Blood Clots Is Impaired in Acute Ischemic Stroke. *Arterioscler., Thromb., Vasc. Biol.* **2017**, *37*, 271−279.

https://dx.doi.org/10.1021/acssensors.0c01596
ACS Sens. XXXX, XXX, XXX−XXX